CONTROLLED SOLIDIFICATION OF FERROSILICON

E. Ott and L. Arnberg

Department of Materials Technology, Norwegian University of Science and Technology,
Trondheim, Norway. E-mail: Emmanuelle.Ott@material.ntnu.no and Lars.Arnberg@material.ntnu.no

ABSTRACT

The microstructure of ferrosilicon is important since it controls the disintegration of the material during crushing and thus the generation of fines. Therefore a study of the microstructure formation during solidification of pure FeSi(75wt%Si) and FeSi(75wt%Si) containing 1.2wt%Al and 0.2wt%Ca has been initiated.

The material has been cast into rods of 8mm diameter, which have been remolten by induction heating and directionally solidified in a Bridgman apparatus. This allows the temperature gradient and the growth rate to be controlled independently. The temperature history during solidification has been recorded by a thermocouple in the melt. Growth rates have been varied between 5 and 400µms^{-1} and temperature gradients between 3 and 14˚Kmm^{-1}. The microstructures show a large dependence on the solidification conditions. The crack formation in the alloys has been studied and found to be strongly related to the microstructure.

1. INTRODUCTION

Industrial ferroalloys are used as inoculant materials in cast-iron and as deoxidisers in steel. Casting into iron moulds/sand moulds and layer casting into beds made of fines are the most used casting methods in the industry. These casting processes offer little control of the microstructure of the cast material. In both cases, the next step in the production process is crushing the alloy to a suitable size for the steel industry. Work on process optimisation has illucidated the problem of fines generation during this crushing process. Fines, defined as having a particle size under 10mm, are likely to be trapped in the slag, while coarser materials would need a longer dissolution time. Thus fines resulting from any crushing process, can be sold only to a limited extent or at a low price.

Many investigations have shown that the crushability of ferroalloys depends on the cooling rate of the cast alloy and on its macro and microstructure [1]-[5]. Some authors have also studied the microstructure as a function of the cooling rate. These studies were based on cooling rates obtained with different industrial casting processes and with laboratory equipment [5]-[7]. The cooling rate was measured but not always controlled. Thus the aim of the present study is to do controlled solidification experiments in order to investigate how the microstructure is influenced by the independent variation of each of the two parameters constituting the cooling rate, the temperature gradient and the growth rate. Two different ferrosilicon alloys have been investigated: the first one is an alloy containing pure silicon (75wt%) and pure iron (referred to FeSi75) and the second one is ferrosilicon (75wt% silicon) with 1.2wt% Al and 0.2wt% Ca (referred to FeSi75(Al, Ca)).

2. EXPERIMENTAL WORK

2.1 Equipment

A Bridgman furnace has been used in order to allow for a certain uncoupling of the growth rate and the temperature gradient. Such a furnace has a hot and a cool zone as seen in Figure 1. The distance between these zones and their temperatures determines the temperature gradient. A crucible is translated through this temperature field at a uniform rate (growth rate).

Proceedings: Tenth International Ferroalloys Congress; 1 – 4 February 2004
INFACON X: '*Transformation through Technology*' Cape Town, South Africa
ISBN: 0-9584663-5-1 Produced by: Document Transformation Technologies

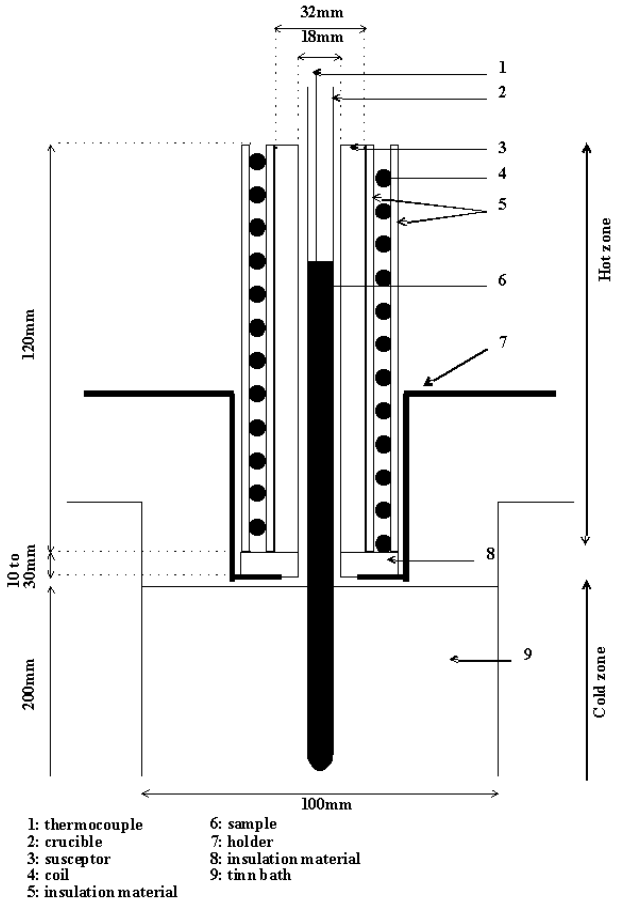

Figure 1. Schematic drawing of the Bridgman furnace.

The heater is made of an induction coil connected to a 12 kW high frequency generator. The frequency varies from 500 kHz to 1,3 MHz depending on the dimensions and the physical properties of the workpiece and has not been measured in this study. Indirect induction heating has been achieved by surrounding the sample by a susceptor. The susceptor consist of a $MoSi_2$ tube with the same length as the coil inside which it is placed. It is believed that the susceptor absorbs all the power of the induction field thereby efficiently shielding the sample as it is heating it. The penetration depth of the induction field has been calculated to be 0,5mm and the thickness of the susceptor is about 12 mm (Figure 1).

The cooler is a tin bath placed a few centimetres below the susceptor and set at 300^{o}C. The free surface is large enough to avoid a significant change in the level of the tin and so to avoid change in the distance between the hot and the cold zone.

2.2 Casting

The sample is molten in the hot zone of the furnace and solidifies before it enters the cold zone. Samples are typically 20 cm long and have a diameter of 8 mm. They are prepared from a mixture of solar-grade silicon and pure iron that are molten by induction heating in a graphite crucible, and then cast by sucking into quartz glass tubes by vacuum. Pure calcium and pure aluminium are added for the impurity containing ferrosilicon. The carbon contamination of the sample is estimated to be below 0,012wt% C at 1820 °K according to previous work [8].

The crucible in the Bridgman furnace is a quartz tube about 40cm long. The inside of this tube is coated with a silicon nitride layer, applied as a water based emulsion which is then dried at 900 °C for an hour. The coating prevents any reaction between the quartz and ferrosilicon. The crucible is connected to an argon inlet and to a vacuum pump. Since ferrosilicon is expanding when solidifying, the tube cracks during the experiment, which is actually without influence on the casting.

The thermocouple is inserted into the melt from the top. A quartz capillary coated with boron nitride protects the lower part. The thermocouple used is of S-type with a platinum sheath and has a diameter of 1 or 1,5 mm. A data logger records the temperature in the sample during the casting experiments.

The crucible is mounted to a screw that moves the system up and down. The rotation of the screw is controlled by a step motor that is itself controlled by a PC program. The speed of the crucible can be regulated down to one $\mu m.s^{-1}$.

When the sample has been placed in the crucible, the whole system is evacuated (4-6 Pa) and back filled with argon. This procedure is carried out several times. The metallic sample is placed in the coil and molten. The crucible is then partially lowered until 1-2 cm of the molten sample is in the tin bath. The thermocouple is inserted in the melt until the tip reaches the middle of the melt. When a stable temperature field is obtained, the crucible is lowered at the desired speed. The thermocouple moves with the sample so that it stays in the same place in the sample during the whole experiment.

2.3 Investigation

The resulting rods have been prepared for metallographic investigation by casting into resin support, ground so that the surface to be studied is a longitudinal cross-section through the centre of the sample, and then polished. They have been observed both by light optical microscopy (microscope I) and scanning electron microscopy. An image analysis software applied on light optical microscope pictures obtained by a different microscope (microscope II) has been used to measure the distance between cracks, the primary silicon grain size and the fraction of pores.

3. RESULTS AND DISCUSSION

A good control of the temperature gradient has been achieved. Both the distance between the hot and the cold zone and the superheat in the melt have been varied to obtain a variation of the temperature gradient. The resulting gradients calculated from the measured distance between the liquidus and the solidus isotherms varied from 3 to $14^{o}K.mm^{-1}$. The growth rate, assumed to be equivalent to the travel velocity of the crucible, has been set to 5, 25, 200, 400 and 800 $\mu m.s^{-1}$ (the last value has been used only for FeSi75 without impurities). One sample has been cast at $200\mu m.s^{-1}$ and then quenched. The rapid change of growth rate lead to a change of the eutectic microstructure allowing observation of the shape of the eutectic growth front. The front has been found to be planar and horizontal as shown in Figure 2.

The image analyses have been carried out at two magnifications (25x and 100x). The lowest magnification is probably better for the evaluation of the primary silicon grains since whole grains are contained in each picture. The highest magnification is probably better to evaluate the distance between cracks since more cracks are visible.

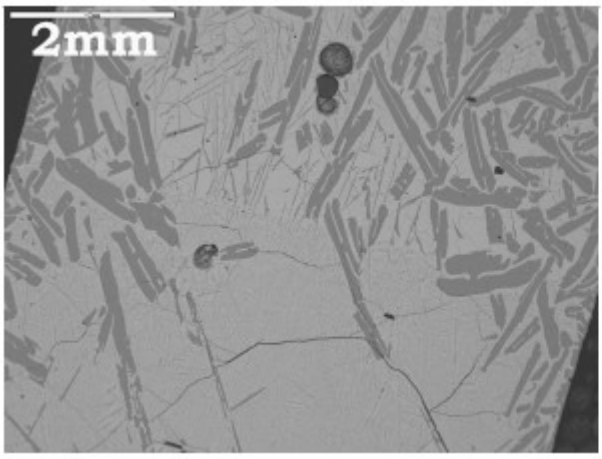

Figure 2. SEM micrograph of the quenched sample showing the planar eutectic front.

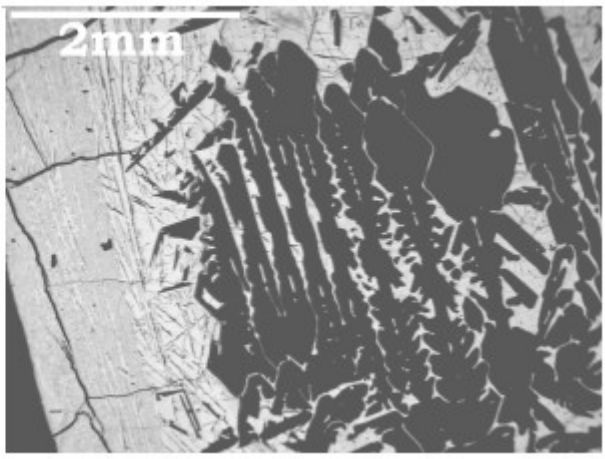

Figure 3. SEM micrograph of a sample with eutectic segregation to the left in the picture and macrocracks.

3.1 Primary silicon grains

A clear change of the primary silicon grain shape has been observed when varying the process parameters. A decreasing growth rate leads to a coarsening of the primary silicon grains and disappearance of the typical two parallel plates growth (Figure 4 and 5). That is actually in contradiction with some previous work where the typical two parallel shape has still been observed in a casting done with a cooling rate in the mushy zone of $3.5.10^{-3}$ $^{o}K.s^{-1}$ [7]. The influence of the temperature gradient is obvious for the samples cast at 200 and 400µm.s^{-1}. A better directionality, longer and fewer grains are observed at higher gradient, which might be explained by the much more narrow mushy zone (Figure 6 and 7). The influence of the gradient at low growth rate is very limited. The presence of aluminium and calcium did not seem to influence the shape of the primary silicon grains.

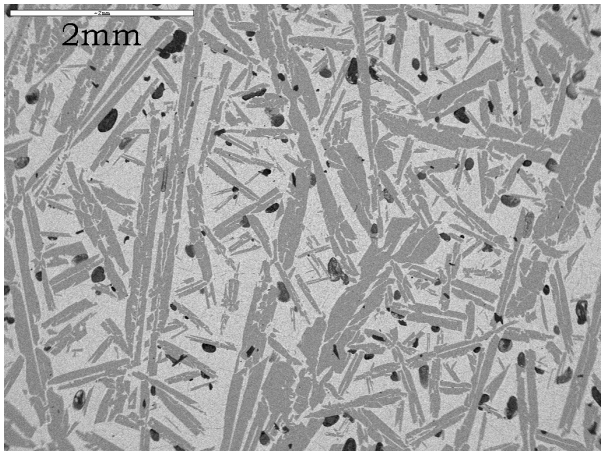

Figure 4. SEM micrograph of a sample cast at 400µm.s^{-1} and high temperature gradient

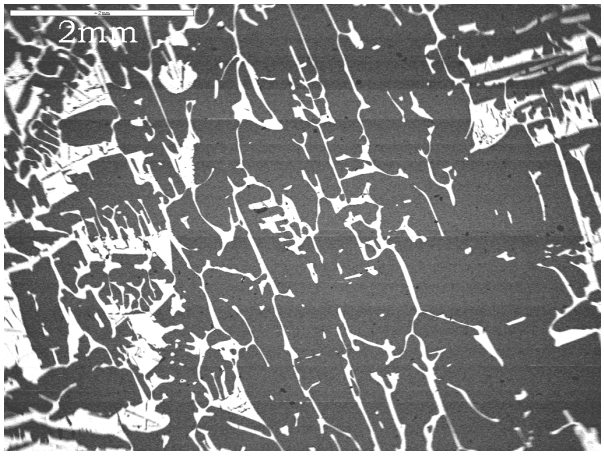

Figure 5. SEM micrograph of a sample cast at 5µm.s^{-1} and high temperature gradient. The primary silicon grains are larger and shorter than at higher growth rate.

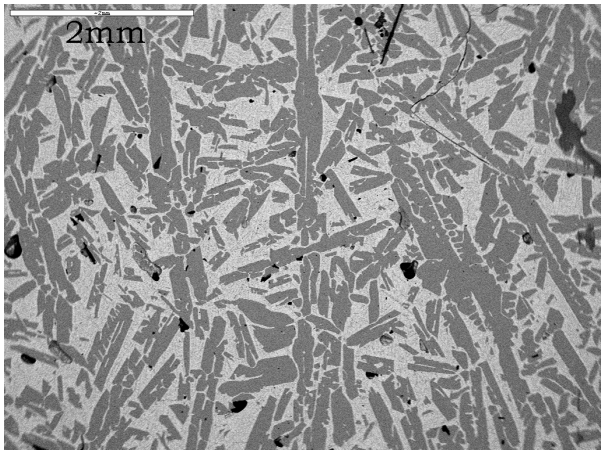

Figure 6. SEM micrograph of a sample cast at 200µm.s^{-1} and low temperature gradient.

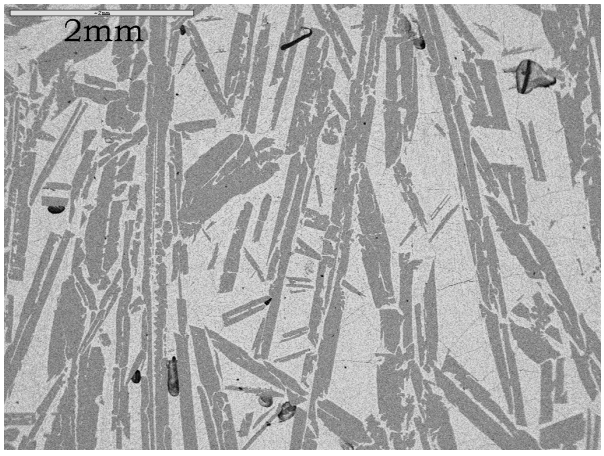

Figure 7. SEM micrograph of a sample cast at 200µm.s^{-1} and high temperature gradient. The primary silicon grains are much longer than at low gradient.

The image analysis concerning primary silicon shows that decreasing the growth rate from 400 to 200µm.s^{-1} hardly influences the size of the grains, while a further decrease leads to a larger grain size (Figure 8). It seems that a higher temperature gradient also results in a larger grain size, which was not obvious from the observation in the SEM.

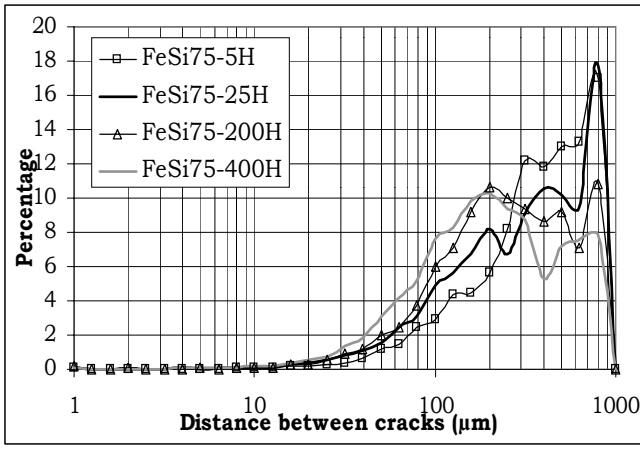

Figure 8. Silicon grain size distribution for samples cast at high temperature gradient and different growth rate. The samples are observed at magnification 25.

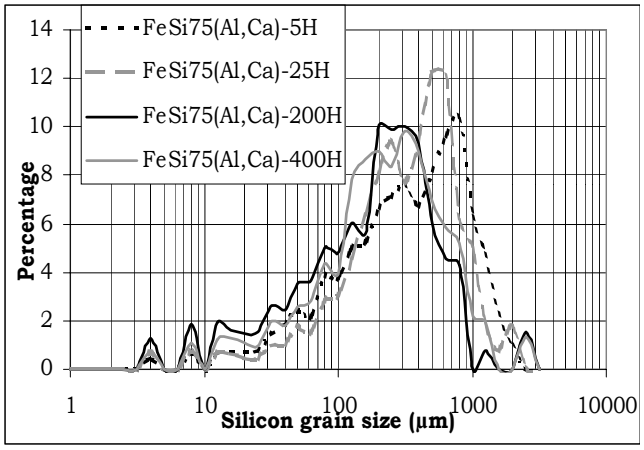

Figure 9. Distance between cracks in samples cast at high gradient and different growth rate. The samples are observed at magnification 100.

3.2 Eutectic

The eutectic microstructure has been found to vary significantly. FeSi75 is first considered. Eutectic in the sample cast at 800µm.s^{-1} is rather dispersed generally but is coupled in some areas. Cells of intermetallic surround the primary silicon grains (Figure 10). In the samples cast at 400µm.s^{-1}, the growth is coupled and tends to be lamellar and finer than for 800µm.s^{-1}. A thin layer of intermetallic surrounds the primary silicon grains (Figure 11). The temperature gradient seems to influence the eutectic growth for the samples cast at 200µm.s^{-1}. The eutectic is finer and less lamellar at higher gradients. The intermetallic layer, almost non-existent at high gradient becomes larger and cellular at lower gradient. The eutectic observed in the samples cast at lower growth rates shows large differences in the same sample. That suggests that the heat flow is varying significantly in a same sample and that it may be influenced by the primary silicon grains. Between the primary silicon grains, eutectic tends to be dispersed while it is finer and lamellar in the segregated part (Figure 3). In FeSi75(Al, Ca), the eutectic is always dispersed (Figure 12) with two exceptions, the sample cast at 200µm.s^{-1} and high gradient (Figure 13) and the eutectic segregated part in the sample cast at 25µm.s^{-1} and low gradient. The intermetallic cells seem to nucleate between the primary silicon grains and grow parallel to the heat direction. Secondary silicon seems to grow between these intermetallic cells leading sometimes to protuberances on the primary silicon grains. Comparing the two samples cast at high growth rate and high temperature gradient shows that the eutectic is much coarser and less plate-like when the sample contains impurities (Figure 11 and 13). This influence of aluminium and calcium suggests that one or both of these elements influence the growth mechanism of eutectic silicon.

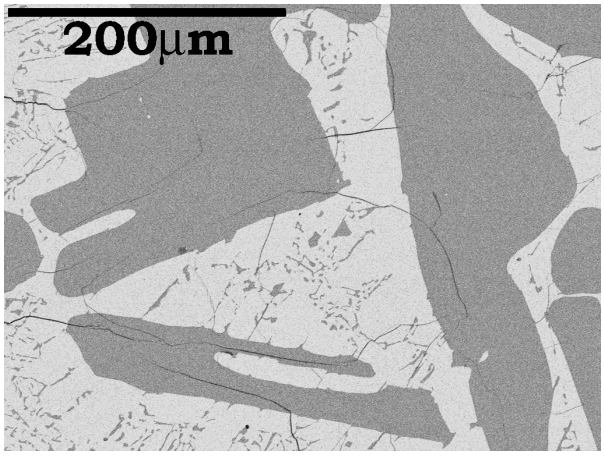

Figure 10. SEM micrograph of a sample cast at 800µm.s^{-1}. Cells of intermetallic are growing around the primary silicon grains.

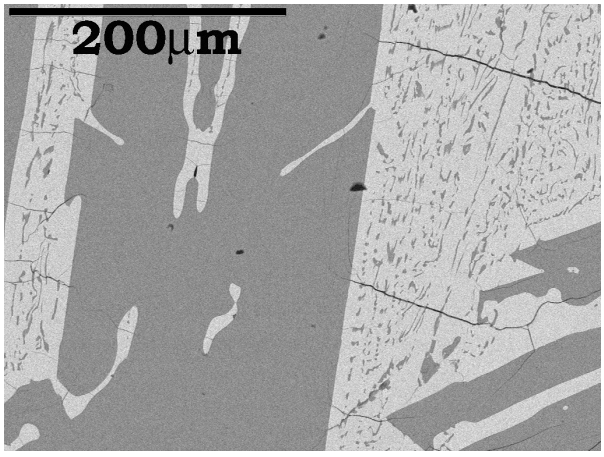

Figure 11. SEM micrograph of a sample cast at 400µm.s^{-1}. The intermetallic layer around the primary silicon grains is rather thin.

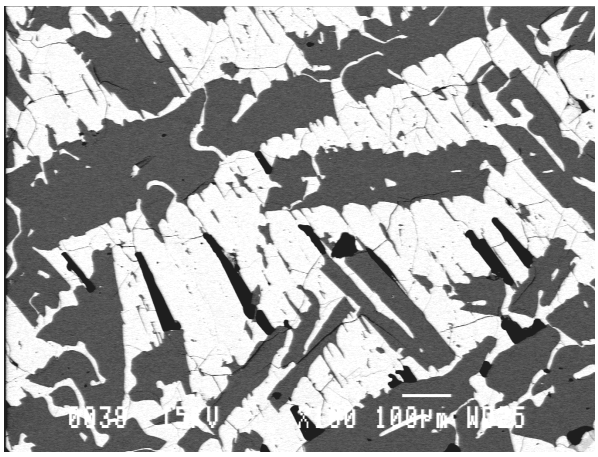

Figure 12. SEM micrograph of a sample containing Al and Ca, cast at 400µm.s^{-1}. The eutectic is dispersed.

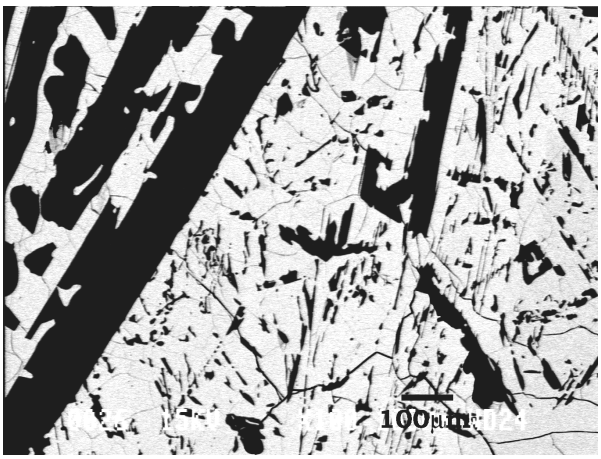

Figure 13. SEM micrograph of a sample containing Al and Ca, cast at 200µm.s^{-1}. The eutectic is coarser than for a sample without Al and Ca but is not really dispersed.

3.3 Distribution of aluminium and calcium

Elemental mapping in an electron micro-probe has been carried out to determine the distribution of the additional elements Al and Ca. The calcium distribution could not be analysed probably because of a too low concentration. The aluminium distribution has been found to be dependent on the growth rate and is probably related to the growth of the intermetallic cells. In the samples containing very clear intermetallic cells, aluminium is segregated on the boundaries of these cells (Figure 14). At low growth rate, aluminium seems to be more soluble in the intermetallic (Figure 15). In any case, the solubility in silicon is very low and not detected by this method.

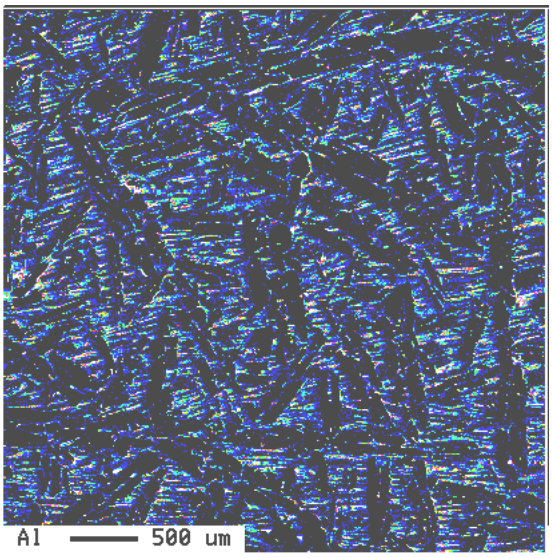

Figure 14. Element map showing the partition of aluminium in a sample cast at 400µm.s^{-1}.

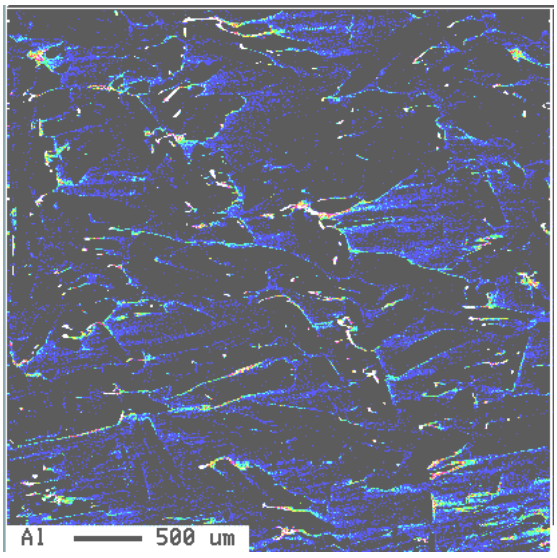

Figure 15. Element map showing the partition of aluminium in a sample cast at 25µm.s^{-1}.

3.4 Cracking

Macrosegregation has been observed in the samples cast at low growth rate, especially at 5µm.s^{-1}. A rather large area containing only eutectic appeared along the edge of the rods. It contains macrocracks visible at low magnification as shown in Figure 3. This agrees with the theory that cracks are induced by thermomechanical stresses resulting from the difference in the coefficient of thermal expansion between silicon and intermetallic [5]. In Figure 3, the left part and the right part of the sample have probably a different expansion coefficient putting the left part under tensile stress.

Observation of the samples by a light optical microscope at magnification 50 shows a variation of the crack pattern. The crack pattern seems to be strongly related to the distribution of the primary silicon grains (Figure 16 and 17). Significantly more cracks can be observed in a sample where the primary silicon grains are highly branched or in high number and randomly oriented. In the samples containing few long and oriented primary silicon grains, the network of cracks is much less dense.

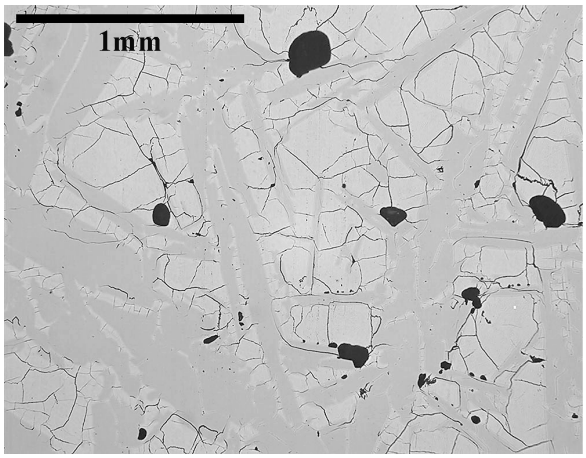

Figure 16. Light optical microscope picture from a sample cast at 400µm.s^{-1} showing the crack pattern.

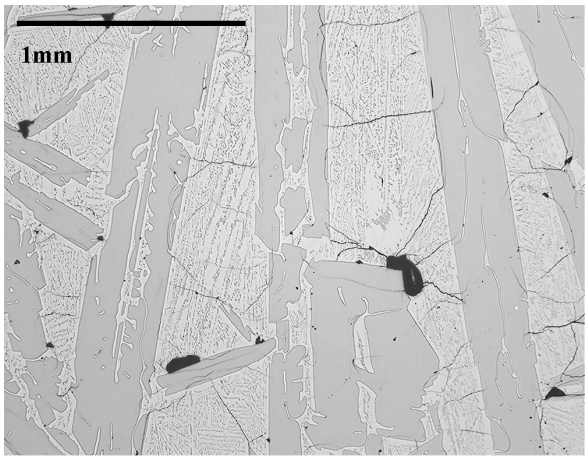

Figure 17. Light optical microscope picture from a sample cast at 200µm.s^{-1} showing the crack pattern.

The image analysis concerning cracks shows that the tendency is an increase of the distance between cracks with the decrease of the growth rate (Figure 9). It is consistent with the tendency observed for the primary silicon grain size, which would suggest that most of the cracks propagate in the eutectic. However, it has been found in some samples that cracks also propagate in silicon (Figure 10) and cracks are usually parallel to the length of the silicon grain. It seems also that some silicon grains resist more to crack spreading than others do. Another explanation for the lower amount of cracks at lower growth rate is the shape of the primary silicon grains. Indeed, round grains would be expected to result in lower local stress than grains with sharp edges. The influence of the growth rate observed with the microscope II and quantified by image analysis does not reflect the influence observed in the microscope I (magnification 50). Observation with microscope I clearly showed for example that the crack network is much denser in the FeSi75 sample cast at 400µm.s^{-1} than in the one cast at 200µm.s^{-1} (Figure 16 and 17). Since the results of the image analysis are similar at magnification 25 and 100, it is probable that the quality of the picture from microscope I is low and that only major cracks are seen. It is uncertain if all the cracks have the same influence on fine generation. At low magnification the typical distance between cracks is between 100 and 1000µm, while it is between 500 and 2000µm at higher magnification. In both cases, the values are higher than the ones found by Guéneau et al. [5], who obtained 30 to 120µm as typical values for the size of the grains delineated by the cracks in the matrix of a high purity ferrosilicon alloy 65wt% Si. The temperature gradient has no influence for the samples cast at high growth rate but a higher gradient leads to a higher distance between cracks at low growth rate. The influence of aluminium and calcium both on the primary silicon grain size and the distance between cracks is very limited.

3.5 Porosity

The growth rate and the alloying elements influence the fraction of pores (Figure 18). At higher growth rate, the porosity increases. The samples cast at 200 and 400µm.s^{-1} actually contain gas pores. When the samples contain aluminium and calcium, the porosity tends to be higher especially at higher growth rates. These samples contain some gas porosity but most of the pores are polishing artefacts that could not be avoided. It has been observed during the sample preparation that samples with aluminium and calcium are much more difficult to prepare. That could be related to the very coarse or dispersed eutectic that results sometimes in relatively large areas with pure intermetallic that is brittle. However, the particles falling out could also correspond to another phase. The pore size is typically between 50 and 200µm.

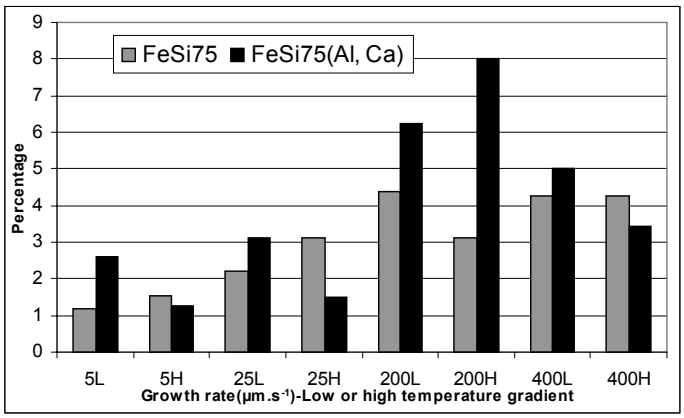

Figure 18. Percentage of pores as a function of the growth rate, the temperature gradient and the composition of the alloys.

4. CONCLUSIONS

Casting two ferrosilicon alloys with controlled process parameters and analyses of the microstructures of the cast samples led to a better understanding of the microstructure formation. Observations made seem to confirm that cracks are induced by thermomechanical stresses resulting from the difference in the coefficient of thermal expansion of silicon and intermetallic.

A decrease of the growth rate mostly influences the microstructure at low growth rates. It results in a coarsening of the primary silicon grains and of the eutectic and an increase of the distance between cracks. An increase of the temperature gradient significantly influences the primary silicon shape at higher growth rates but not at lower growth rates. It results in a higher distance between cracks at low growth rates but does not have influence at higher growth rates.

Aluminium and calcium do not influence the shape of the primary silicon grains but lead to a very coarse or dispersed eutectic. The silicon grains seem to inhibit cracks' spreading but do not necessarily stop them. The crack network seems strongly dependent on the microstructure of primary silicon. Samples containing aluminium and calcium seem to be more brittle, which might be attributed to the dispersed eutectic.

5. REFERENCES

[1] Vicintin, R.A., Silveira, R.C., Zepeda, S.; "Geração de finos na produção dos FeSi 75%", Instituto Latinoamericano del Fierro y el Acero. Casilla 16065, Siantago 9, Chile 1982. Conference. Ferroaleaciones 82, Rio de Janeiro, Brazil, 1982.

[2] Marguarido, F., Martins, J.P., Gon Alves, A., Figueiredo, M.O.; "Microstructure vs. casting processes in the Fe-Si-Ca-Al system", Mat. Sci. and Eng. A, A173, 1993, pp115-118.

[3] Sigfusson, T.I., Mathiasson, J., Ingason, H.T., Sigurdsson, J.V., Halfdanarson, J.; "A model for layer casting ferrosilicon", Electr. Furn. Conf. Proc., 1993, vol 51, pp187-192.

[4] Aplan, F.F., Kirby G.N., "The influence of structure and properties on the grinding of ferrosilicon", Phys. Chem. Powder Met. Prod. Process, publishers: Miner. Met. Mater. Soc. Warrendale Pa, 1989, pp413-429.

[5] Guéneau, C., Servant, C. and Manier, F., "Relationships between the grinding behaviour and the microstructure of ferro-silicon alloys with 65 wt. % silicon", Infacon VII, publishers: FFF Trondheim Norway, 1995, pp. 673-681.

[6] Mihok, L., Adamus, V.; "Control of common ferroalloys structure", publishers: Hungarian Mining and Metallurgical Society (OMBKE) Budapest Hungary, 1994, pp621-625.

[7] Tveit, H., "Størkning av 75% ferrosilisium, foløp, struktur og styrke", Ph.D. Thesis, Institute for Materials Science, Norwegian University of science and Technology, trondheim, Norway, 1988.

[8] Ottem, L., "Løslighet og termodynamisk data for oksygen og karbon i flytende legeringer av silisium og ferrosilisium", SINTEF report, 1993.